Renal Cysts of *inv/inv* Mice Resemble Early Infantile Nephronophthisis

CARRIE L. PHILLIPS,*† KAREN J. MILLER,† ADELE J. FILSON,* JENS NÜRNBERGER,* JEFFREY L. CLENDENON,* GREGORY W. COOK,* KENNETH W. DUNN,* PAUL A. OVERBEEK,‡ VINCENT H. GATTONE II,§ and ROBERT L. BACALLAO*

*Department of Medicine, *Division of Nephrology and †Department of Pathology, and §Department of Anatomy and Cell Biology, Indiana University School of Medicine, Indianapolis, Indiana; and ‡Department of Molecular and Cellular Biology, Baylor College of Medicine, Texas Medical Center, Houston, Texas.*

Abstract. Cystic kidney disease has been linked to mutations in the *Invs* gene in mice with *inversion of embryonic turning* (*inv/inv*) and the *INVS* (*NPHP2*) gene in infants with nephronophthisis type 2 (NPHP2). The *inv* mouse model features multiorgan defects including renal cysts, altered left-right laterality, and hepatobiliary duct malformations transmitted in an autosomal recessive manner. Affected mice usually die of renal and liver failure by postnatal day 7. Although cardiopulmonary and liver anomalies have been carefully detailed, renal cysts have yet to be fully characterized in *inv/inv*. By use of three-dimensional visualization by two-photon microscopy, this study provides the first comprehensive analysis of *in situ* cyst formation and progression in *inv/inv* kidneys. At embryonic day 15, there is dilatation of Bowman's capsule followed temporally by corticomedullary cysts involving collecting ducts, proximal tubules, and thick ascending limbs. Collecting ducts of newborn *inv/inv* mice are uniformly and diffusely cystic from medulla to cortex, with normal diameters found only at their most proximal tips. Proximal tubules form fusiform cysts that alternate with segments of normal or narrowed caliber along torturous convolutions. Because defective cilia have been linked to *situs inversus* and cystogenesis, we examined *inv/inv* cilia by scanning and transmission electron microscopy. The former detected monocilia of expected length in cystic collecting ducts and proximal tubules; the latter demonstrated the usual 9 + 2 pattern in respiratory cilia. The *inv* mutant mouse has renal cysts resembling infantile NPHP2 and will provide broader insight into the role cilia play in renal cystogenesis.

Inherited cystic kidney diseases comprise a large category of disorders characterized by cystic kidneys and multiorgan pathology. Both autosomal recessive and autosomal dominant patterns of transmission have been described in humans and murine models (1). Regardless of the gene defect in humans, cystic expansion of epithelial-lined renal tubules leads to progressive loss of renal function and eventual dependence on dialysis or transplantation. Autosomal dominant polycystic kidney disease (ADPKD) is symptomatic in adulthood and attributed to mutations in the *PKD1* gene encoding polycystin-1, and *PKD2* encoding polycystin-2 (2). A number of gene mutations have been recently described in infants and children with renal cysts (3) including *PKHD1* underlying autosomal recessive polycystic kidney disease (ARPKD) (4,5), *NPHP1* in juvenile NPHP1 (6), *INVS* in infantile nephronophthisis type 2 (NPHP2) (7), *NPHP3* in adolescent NPHP3 (8), and *NPHP4* in a second juvenile form (9). Although a complex cascade of proteins is known to influence tubulogenesis (10) and maintain normal renal function, less is understood about how certain gene mutations initiate cystogenesis.

Renal cysts arise from unchecked proliferation of epithelial cells, loss of epithelial cell polarity, and defects in epithelial communication with an altered extracellular matrix (11–13). These perturbations may be explained, in part, by disruption of calcium homeostasis that is normally maintained when polycystin-1 and -2 interact to regulate cation channels (2). The interaction of polycystins with *NPHP* gene products is unknown but the answer may be found in cilia and junctional complexes. Flow generated by motile cilia in the embryonic node appears to establish the left-right vertebrate axis (14), whereas nonmotile, primary cilia on the apical surface of renal tubular cells are postulated to act as mechanosensory receptors (15). Primary cilia may detect changes in urine flow or content and transmit signals to junctional complexes to regulate epithelial cell differentiation. Inversin, the product of *Invs*, has recently been found in cilia (16,17) as have other cyst-associated proteins including cystin (18), polaris (19), polycystin-1 and -2 (20,21), fibrocystin (4), and nephrocystin (7), adding further evidence to the postulated role of defective cilia assembly as a proximate cause of renal cysts. A relationship between

Received November 29, 2001. Accepted April 19, 2004.

Correspondence to Dr. Carrie L. Phillips, Indiana University School of Medicine, Department of Medicine, Division of Nephrology, 950 West Walnut, R2-202, Indianapolis, IN 46202-5188. Phone: 317-274-1266; Fax: 317-274-8575; E-mail: cphilli3@iupui.edu

1046-6673/1507-1744
Journal of the American Society of Nephrology

DOI: 10.1097/01.ASN.0000131520.07008.B3

cilia and junctional complexes is suggested by colocalization of polycystin-1 with E-cadherin and the catenins (22), inversin with N-cadherin and the catenins (23), and nephrocystin with inversin (7).

Development of animal models that reliably mimic human disease will facilitate the study of cyst-associated proteins in organelles such as cilia. *Invs* is one of several murine genes associated with renal cysts, but *inv/inv* mice were also reported to have alterations in left-right asymmetry, cardiovascular defects, an anomalous hepatobiliary system, and premature death (24–29). Although *INVS* has been sequenced and mapped in humans (as *NPHP2*) (7,30) and mice (as *Invs*), the function of inversin is unknown.

Initial reports of the *inv* mutant model noted renal cysts in two-dimensional (2-D) histologic sections of newborn kidneys shown at relatively low magnifications. Kidneys of affected newborn mice were described as having "severely dilated collecting ducts," whereas heterozygotes had no phenotypic abnormalities (24,27). Morgan *et al.* (17) reported normal appearing monocilia in kidneys but did not designate the tubule segment. We carefully studied *inv* mutants as a model of early infantile nephronophthisis and characterized renal changes from embryonic through postpartum development by use of bright-field and electron microscopy and two-photon fluorescence microscopy with three-dimensional (3-D) analysis.

To understand the genesis of renal cysts, we used two-photon microscopy and digital image processing to generate 3-D images of *in situ* cysts. Compared with confocal microscopy, two-photon microscopy more efficiently collects scattered fluorescence without significant photobleaching of fluorescently labeled, thick biologic specimens (31). Because fluorescence probes may be targeted to specific renal molecules, two-photon technology is ideal for determining the relationship of renal cysts to contiguous and adjacent nephron segments and surrounding matrix. 3-D images produced by volume-rendering software that uses two-photon data are less labor intensive in acquisition and offer more information than microdissection or conventional 2-D techniques (32–34).

Materials and Methods

Animals

Handling of mice conformed to institutional animal care guidelines established by the National Institutes of Health. After halothane inhalation and nuchal dislocation, a laparotomy was performed on pregnant mice, and embryos were removed at days E15 or E17 and fixed in 10% buffered formalin for histology. Kidneys harvested from newborn mice at postpartum day 1 (P1), day 5 (P5), and day 11 (P11) were fixed in 10% buffered formalin (Fisher Scientific, Fair Lawn, NJ) for bright-field microscopy. Day P2 to P5 kidneys were immersion-fixed in 4% paraformaldehyde (Fisher Scientific) for two-photon microscopy (31). Kidneys and trachea were fixed in 3% glutaraldehyde-formaldehyde in 0.1 M sodium cacodylate (Tousimis, Rockville, MD) for scanning electron microscopy (SEM) or transmission electron microscopy (TEM). Lack of pigmentation in albino control mice (+/+) allowed for phenotypic distinction from homozygotes (*inv/inv*) with *situs inversus*, or heterozygotes (*inv*/+) with intact left-right asymmetry (24,27). Body and kidney weights were collected on a range of newborn mice available at time of study.

Bright-field Microscopy

All formalin-fixed kidneys were embedded in paraffin, sectioned 3 to 4 μm in thickness, and stained with periodic acid–Schiff. 2-D sections were collected with a Leica DMLB microscope (Bannockburn, IL) equipped with a Polaroid DMC digital camera (Bedford, MA). Two kidneys from each animal (*inv/inv, inv*/+ and +/+) were examined at E15 ($n = 2$), E17 ($n = 4$), P1 ($n = 6$), and P11 ($n = 1$). A tubule was deemed cystic if the diameter was twice that of +/+ littermates.

Electron Microscopy

SEM of kidney was performed on an Amray 1000A (KLA Tencor, Bedford, MA). For TEM, thin sections of trachea were examined on a Philips CM10 TE (FEI, Mahwah, NJ). Two *inv/inv* and +/+ animals were examined by each method as described (35).

Immunohistochemistry

Paraformaldehyde-fixed kidneys were Vibratome sectioned up to 200 μm thick (Technical Products International, Inc., St. Louis, MO), washed in 1 × PBS, and incubated overnight (4°C) with one or more of the following: (*1*) rhodamine- or fluorescein-labeled lectins (Vector Labs, Burlingame, CA), (*2*) rhodamine-phalloidin (Molecular Probes, Eugene, OR), which labels filamentous (F) actin and/or (*3*) Tamm-Horsfall protein antibody (Biomedical Technologies, Stoughton, MA), to label thick ascending limb of Henle. Fluorescein-goat anti-rabbit (Jackson Immunoresearch, West Grove, PA) was used as secondary antibody for Tamm-Horsfall antibody. Peanut agglutinin (PNA) and *Dolichos biflorus* (DBA) lectins label collecting ducts. PNA and *Lotus tetragonolobus* (LTG) label proximal tubules. Lectins, phalloidin, and antibodies were diluted 1:200 in 2% BSA, 0.1% Triton X-100, and 1× PBS (Fisher Scientific). After a 4-h wash in 1× PBS, sections were placed on glass coverslips mounted to No. 1.5 culture dishes (MatTek, Ashland, MA). Formalin-fixed, paraffin-embedded, 5-μm-thick sections of newborn kidney (day P1) were deparaffinized through a xylene-ethanol gradient, labeled with DBA lectin followed by anti-DBA antibody, and developed with diaminobenzidine as chromagen (Vector Labs).

Two-Photon Fluorescence Microscopy

Optical sections were collected on a Bio-Rad MRC1024 confocal/2 photon system (Bio-Rad, Hercules, CA) fitted to a Nikon Eclipse inverted microscope with ×20, ×40, or ×60 water-immersion objectives (Nikon, Melville, NY) at the Indiana Center for Biological Microscopy (http://nephrology.iupui.edu/imaging). Illumination was provided by a Spectra-Physics (Mountain View, CA) Tsunami Lite Titanium-Sapphire laser tuned to a wavelength of 800 nm. The objective collar was matched to the coverslip thickness. Data sets were collected as Z-series spaced from 0.4 μm (×60 objective) to 1.0 μm (×20 objective).

Image Analysis

3-D images were produced by Voxx (36), a volume rendering program (available free from http://nephrology.iupui.edu/imaging/voxx). Segmentation and surface rendering of tubule luminal space was performed with Amira (TGS, San Diego, CA). Adobe Photoshop (San Jose, CA) was used to assemble and label final figures. To generate composites of Vibratome kidney sections, neighboring Z-series were collected via two-photon microscopy, rendered in Voxx, saved as TIFF files, and assembled in mosaics by Adobe Photoshop.

Results

Gross Development

inv/inv exhibit *situs inversus* (Figure 1) and usually die within the first week of life, although one pup survived to P11.

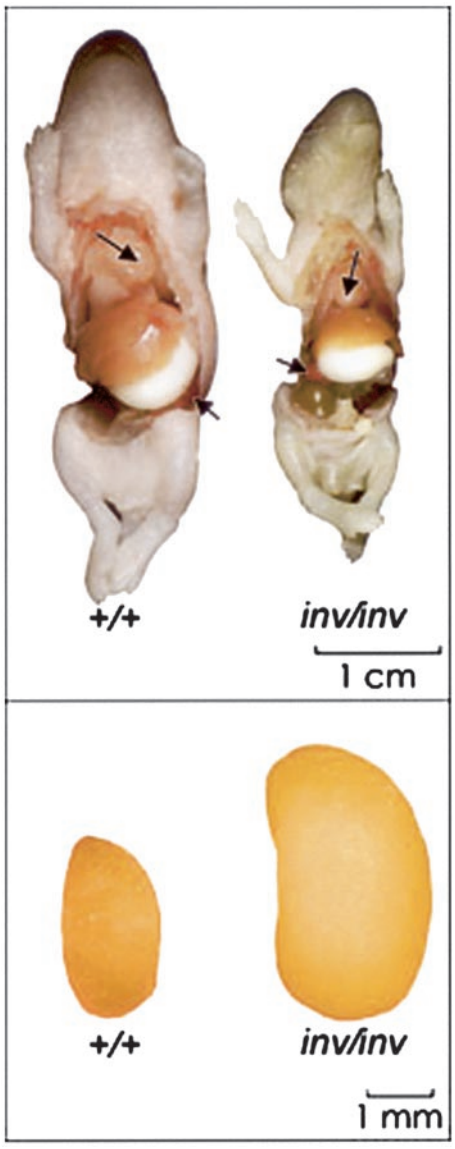

Figure 1. (top) Day P5 wild-type (+/+) and mutant (*inv/inv*) mice. The mutant mouse had decreased body size, yellow discoloration of skin, and cystic kidneys. Spleen (short arrows) and the apex of the heart (long arrows) are on the right side of *inv/inv* and the left side of +/+ littermate. The bottom panel shows larger cystic kidneys of an *inv/inv* as compared with normal-sized kidneys from a +/+ littermate.

+/− mice followed up to 1 yr do not exhibit significant gross abnormalities (data not shown). Compared with age-matched +/+ littermates, *inv/inv* mice showed poor body growth, jaundice and developed progressively enlarging renal cysts (Figure 2). By day P5, *inv/inv* mice were azotemic with twice the concentration of blood urea nitrogen as compared with unaffected (+/+ and +/*inv*) littermates (data not shown).

Light Microscopy

We inspected 2-D histologic sections of formalin-fixed, paraffin-embedded kidneys from embryonic (days E15, E17) and postpartum (days P1, P11) mice with bright-field microscopy. Relatively rapid development and progression of epithelial-lined cysts were found in nephrons of *inv/inv* mice (Figure 3). Expansion of Bowman's space surrounding deep cortical glomeruli was the earliest defect observed in E15 *inv/inv* (Figure 3B), and this feature persisted through day P11 (Figure 3F). By day E17, cysts began to appear in collecting ducts and proximal tubules (data not shown) and these progressed in size and number in the cortex and medulla of newborn day P1 mice (Figure 3, C and D), whereas kidneys of age-matched +/*inv* and +/+ littermates developed normally (data not shown). Day P11 *inv/inv* kidneys showed diffuse and elaborate cystic expansion of proximal tubules, collecting ducts, and Bowman's space (Figure 3F) that was similar but more extensive than was seen at day P1. A few *inv/inv* tubular lumina (<5%) contained dystrophic calcifications (data not shown). Kidneys from +/+ and +/*inv* kidneys showed densely packed tubules with normal nephron development at day P11 (Figure 3E).

Two-Photon Fluorescence Microscopy and 3-D Rendering. Vibratome sections of paraformaldehyde-fixed newborn mouse kidneys (P2 to P5) were labeled with fluorescently tagged lectins, phalloidin, and/or anti–Tamm-Horsfall. Z-series

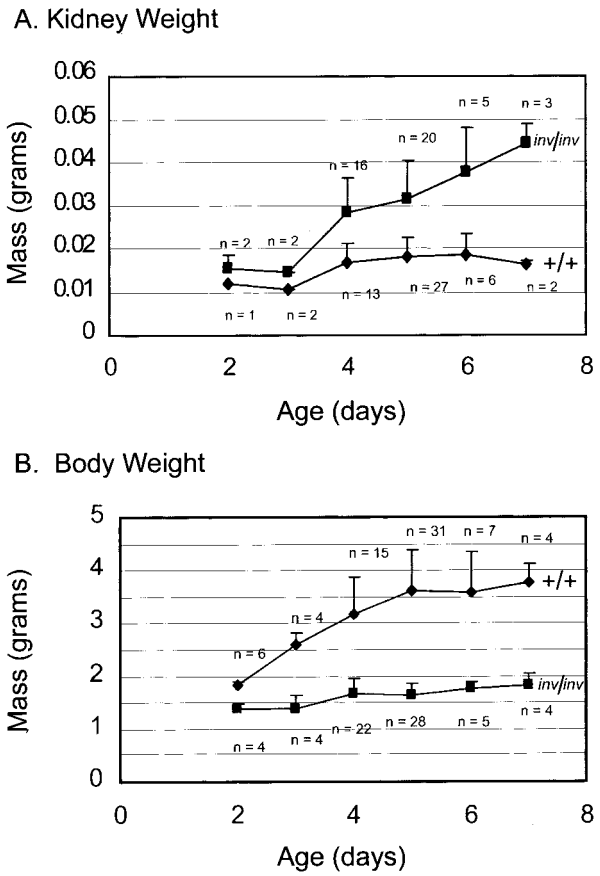

Figure 2. Graphs showing kidney (A) and body (B) mass of *inv/inv* (■) mice compared with +/+ control littermates (♦) during the first week of life. (A) Cystic kidneys of P7 *inv/inv* mice weighed more than twice as much as +/+ kidneys. (B) Body weight of +/+ mice progressively increased whereas little weight gain was noted in *inv/inv* mice (n = number of mice per time point available).

of optical slices from each tissue section were acquired on a two-photon microscope and explored in near–real time by Voxx (Figures 4 through 9).

Single-Channel, Two-Photon Microscopy of Proximal Tubules. In kidneys of P5 +/+ mice, proximal tubules of uniform caliber were found among compact arrays of cortical nephrons labeled with PNA or LTG (Figure 4, A, C and E). These lectins labeled apical brush borders, intracellular vesicles, and basal aspects of epithelial cells in proximal tubules of unaffected mice. A considerably different morphology was found in lectin-labeled cystic kidneys of day P3 and P5 *inv/inv*, which showed fusiform, not sacular, dilatation of convoluted and straight proximal tubules (Figure 4, B, D, and F through H) that were bridged by segments of normal or narrowed calibers (apparent in Figure 4, B and G). Within progressively expanding cysts, the apical brush border microvilli appeared to be either intact or focally thinned. Intact brush borders suggested that epithelial polarity is at least structurally intact in *inv/inv* proximal tubules. Rarified microvilli appeared similar to loose, ill-fitting pieces of jigsaw puzzles (Figure 4D). Fusiform dilatation of collecting ducts was seen with PNA labeling (Figure 4, B and D).

Multicolor, Two-Photon Microscopy, and Segmentation of Proximal Tubules. To analyze proximal tubules *in situ*, Vibratome sections were labeled with two fluorescence markers (Figures 5 and 6). PNA-labeled proximal tubules from *inv/inv* mice showed variable luminal widening and cysts (Figure 5, B through D). The interstitium appeared relatively disorganized and more abundant (Figure 5, B and C) when sections were dual-labeled with phalloidin. Similarly labeled +/+ kidneys had evenly dispersed glomeruli and uniform tubules with little intervening interstitium (Figure 5A).

We used Amira software to determine the luminal pathway within tortuous convoluted proximal tubules (Figure 5, E and F), a task that proved difficult and time-consuming by 2-D

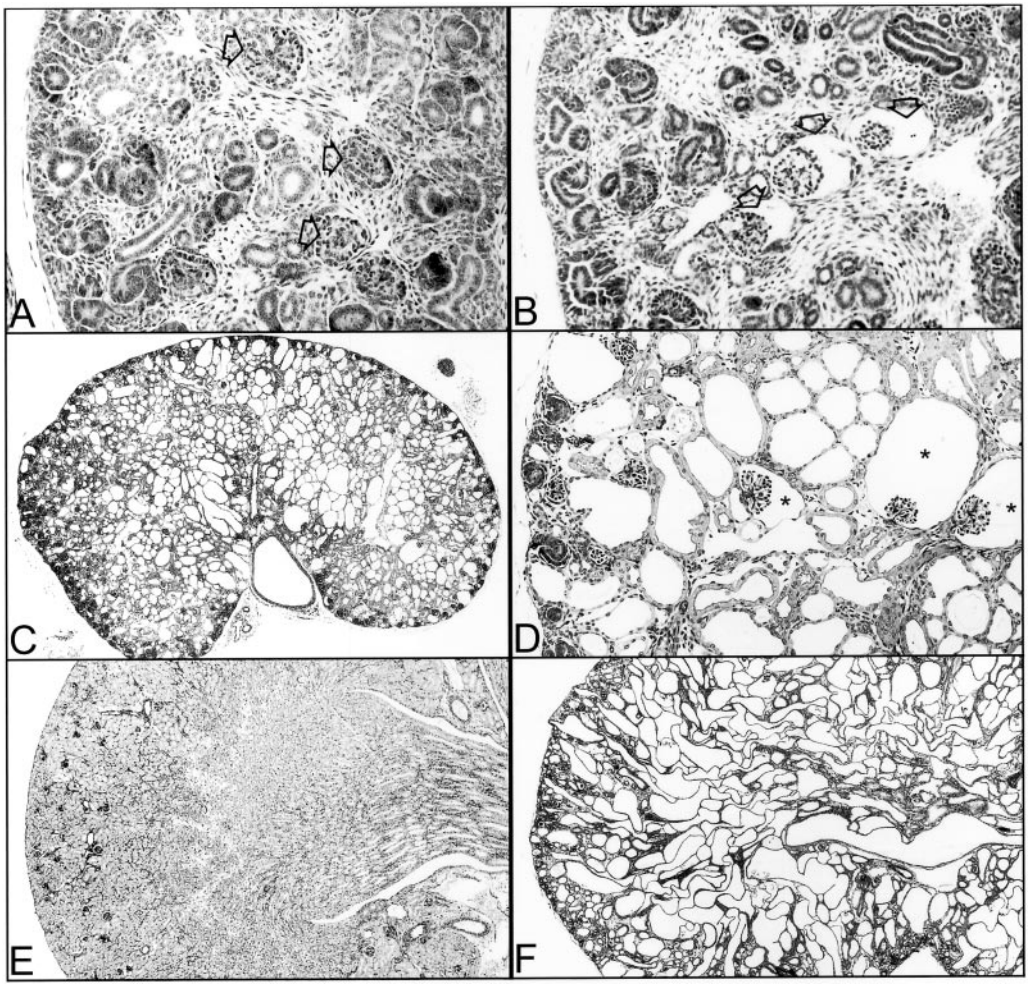

Figure 3. Two-dimensional, bright-field microscopic images of periodic acid–Schiff–stained kidneys. (A) +/+, day E15 (original magnification, ×200). (B) *inv/inv*, day E15 (original magnification, ×200). Expansion of Bowman's space surrounding deep cortical glomeruli (open arrows) was noted in day E15 *inv/inv* kidneys (B) but not +/+ (A). (C) *inv/inv*, day P1 (original magnification, ×40). (D) *inv/inv*, day P1 (original magnification, ×200). Cysts involving collecting ducts, proximal tubules and Bowman's spaces (*) are seen in P1 *inv/inv*. (E) +/+, day P11 (original magnification, ×40). (F) *inv/inv*, day P11 (original magnification, ×40). When compared with the dense parenchyma of +/+ kidney at day P11 (E), *inv/inv* shows diffuse cortical and medullary cysts (F).

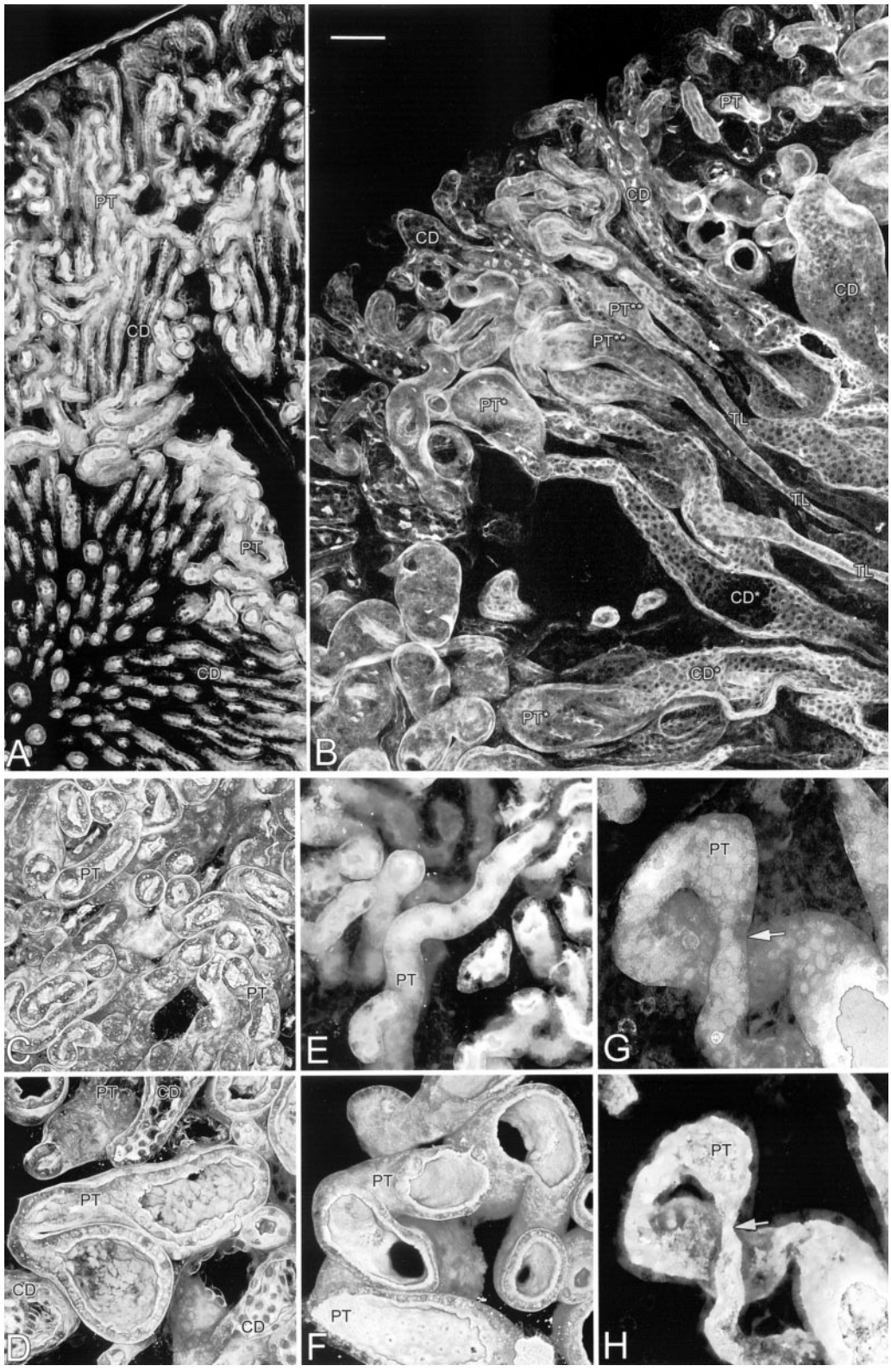

Figure 4. Single-channel, two-photon microscopy and three-dimensional rendering of day P5 proximal tubules (PT), thin descending loops of Henle (TL), and collecting ducts (CD). (A) +/+, PNA lectin, six adjacent Z-series assembled into one image. (B) *inv/inv*, PNA lectin, six adjacent Z-series with longitudinal orientation of tubules. Manual rotation of individual volumes in Voxx distinguished PT and CD that falsely appear connected in nonrotated state (*). Dilated S3 segments of PT (**) narrow distally into TL. Scale bar for A and B = 100 μm. (C) +/+, PNA lectin, 205 μm (x-axis) × 205 μm (y-axis) × 77 μm (z-axis). (D) *inv/inv*, PNA lectin, 205 × 205 × 79 μm. (E) +/+, LTG lectin, 205 × 205 × 42 μm. (F) *inv/inv*, LTG lectin, 205 × 205 × 88 μm. (G and H) *inv/inv*, LTG lectin, 180 × 180 × 66 μm. Surface of PT is rendered opaque in G and transparent in H to visualize attenuated lumen (arrow).

(Figure 5, G through J). The lumen was analyzed, rather than the basal surface, because this space represents the route of urine flow that may be functionally obstructed. We identified normal, cystic, and narrowed regions within the lumen of a single, serpentine tubule. Although disconnected, blind pouches were not identified, there were cystic segments next to markedly narrowed segments that may function like blind pouches (between segments 2 and 4, 5 and 6, or 6 and 7 in Figure 5, D through J). Similar narrowing was detected where S3 segments transitioned to descending thin loops of Henle in the outer medulla, where occasional diverticuli were noted (Figure 6). Rare, small outpocketings were seen along proximal tubules (segment 4, Figure 5D).

Single-Channel, Two-Photon Microscopy of Collecting Ducts. Collecting ducts from *inv/inv* mice were labeled with DBA lectin and imaged by two-photon microscopy (Figure 7).

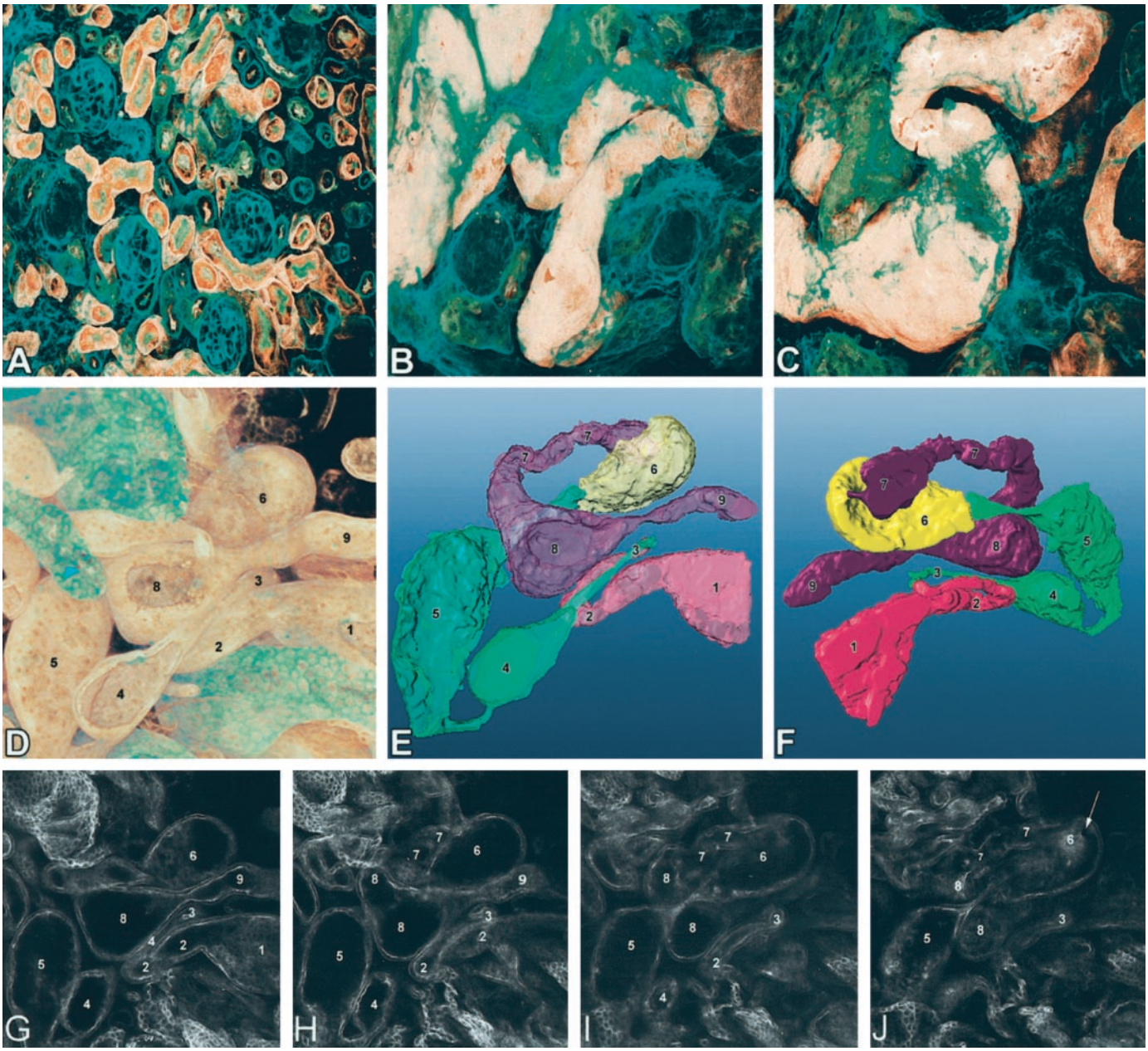

Figure 5. Two-photon microscopy, three-dimensional rendering and segmentation of proximal tubules. (A) +/+, day P5, 205 (x-axis) × 205 (y-axis) × 31 μm (z-axis); (B) *inv/inv*, day P5, 205 × 205 × 29 μm; (C) *inv/inv*, day P5, 205 × 205 × 60 μm. Cystic proximal tubules (PNA-lectin, tan in B and C) were surrounded by relatively abundant F-actin in the interstitium (phalloidin, green in A through C). (E, F) Segmentation with Amira revealed *in situ* fusiform cysts, hairpin turns and narrowed segments in a single day P4 convoluted proximal tubule (tan in D, original volume, 512 × 512 × 91 μm, with DBA-labeled collecting ducts [green]; E = translucent, front view; F = opaque, back view). (G–J) Optical two-dimensional (2-D) slices at 10-μm intervals, taken from the volume rendered in (D), show cysts with narrowed segments (J, arrow). The numbers 1 to 9 in panels D through J allow comparison of 2-D and three-dimensional renderings.

Composites of microscopy volumes showed that *inv/inv* collecting ducts were diffusely expanded up to 20 times the diameter of +/+. The caliber of *inv/inv* collecting ducts approached that of +/+ only at their immature proximal ends in the outermost cortex (Figure 7B). Like +/+, the *inv/inv* collecting ducts maintained their parallel alignment from medulla to cortex. DBA-positive cysts were easily identified by immunoperoxidase (Figure 7, inset); however, the 2-D nature of this technique gives the false impression that cystic collecting ducts are not parallel.

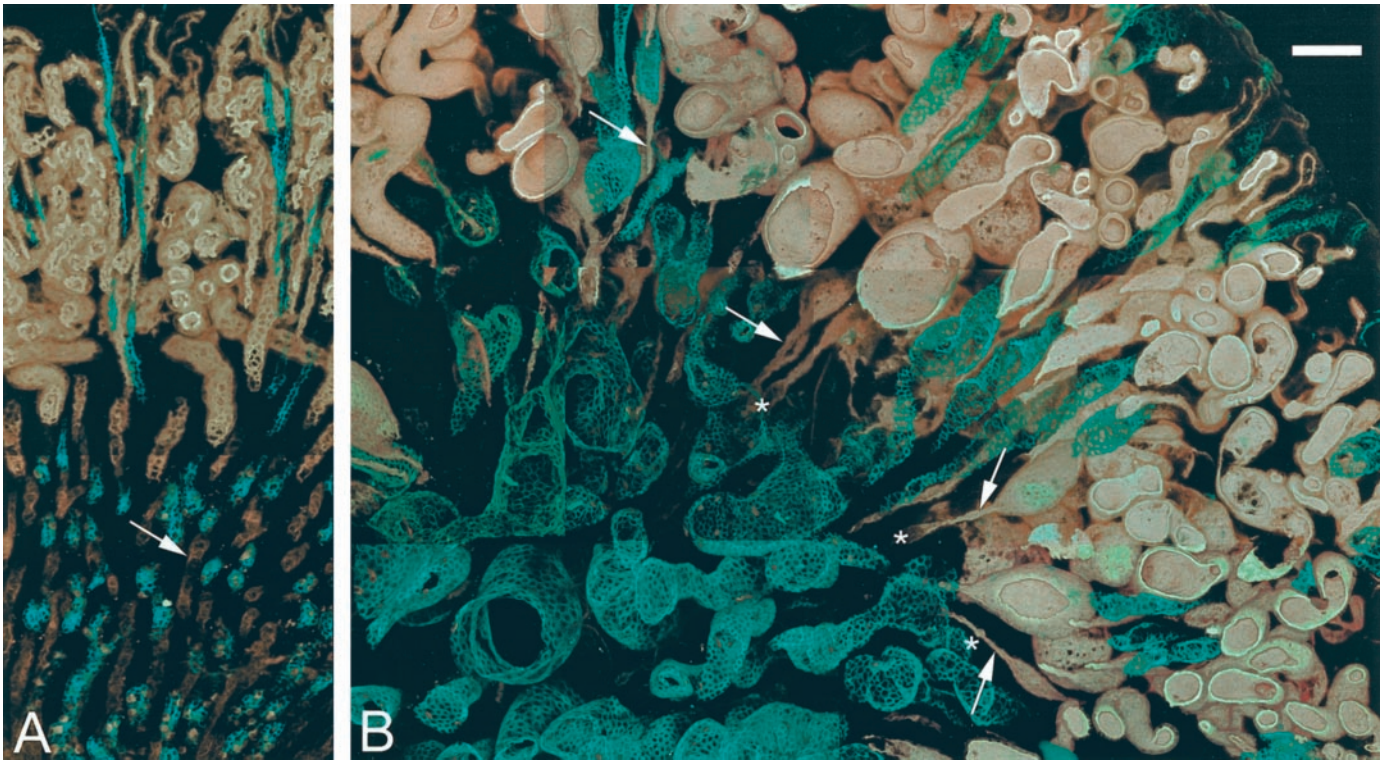

Figure 6. Dual-color, two-photon microscopy and three-dimensional rendering of day P2 +/+ (A) and *inv/inv* (B) show collecting ducts (DBA lectin, green) in relationship to proximal tubules (LTG lectin, tan). Arrows indicate thin descending loops of Henle that in *inv/inv* narrowed at their transitions from S3 segments. Some of these thin loops have diverticuli or flaring at their distal ends (*). A was assembled from 3 adjacent Z-series and B from 12. Scale bar = 100 μm.

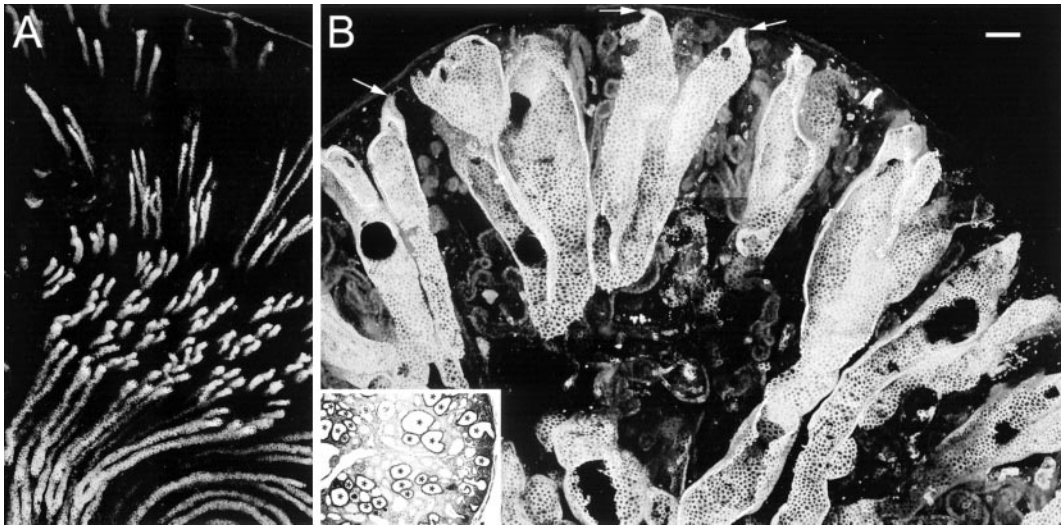

Figure 7. Single-channel, two-photon microscopy with three-dimensional rendering shows longitudinal view of day P5, DBA-positive collecting ducts (B, *inv/inv,* 14 adjacent Z-series) that were diffusely dilated throughout their entire lengths except at proximal tips (arrows). Compare with normal caliber collecting ducts of +/+ (A, eight adjacent Z-series). Scale bar = 100 μm. Inset: immunoperoxidase staining with DBA shows cross sections of dilated collecting ducts (*) in two dimensions (day P1).

Multicolor, Two-Photon Microscopy Shows Heterogeneous Labeling of Collecting Ducts. Figure 8 shows heterogeneous labeling of cysts arising in *inv/inv* collecting ducts that were dual-labeled with DBA and phalloidin, or DBA and LTG lectin. In collecting duct cysts in the outer cortex, there was loss of DBA labeling at many of the proximal tips (Figure 8, B, D, and E). This consistently occurred at the entrance and incorporation of distal tubule cells into the cyst wall, indicating that individual fusiform cysts can affect a region of tubule regardless of tubule segment boundaries. Further heterogeneity was demonstrated when both DBA-positive principal cells and LTG-positive intercalated cells were found in the same collecting duct cysts (Figures 6B and 8C).

Multicolor, Two-Photon Microscopy of Thick Ascending Limbs. In the medulla, anti–Tamm-Horsfall antibody labeled thick ascending limbs that were of normal caliber in +/+ kidneys (Figure 9A) but appeared dilated in *inv/inv* kidneys (Figure 9B).

Scanning and Transmission Electron Microscopy

We used SEM to examine monocilia in renal tubules (Figure 10). In day P5 *inv/inv* kidneys, normal-appearing monocilia were detected at apical surfaces of cystic collecting ducts (Figure 10C) and proximal tubules (Figure 10D). By use of high-resolution TEM, we examined respiratory cilia from trachea of *inv/inv* mice (Figure 10E). Within the axoneme mem-

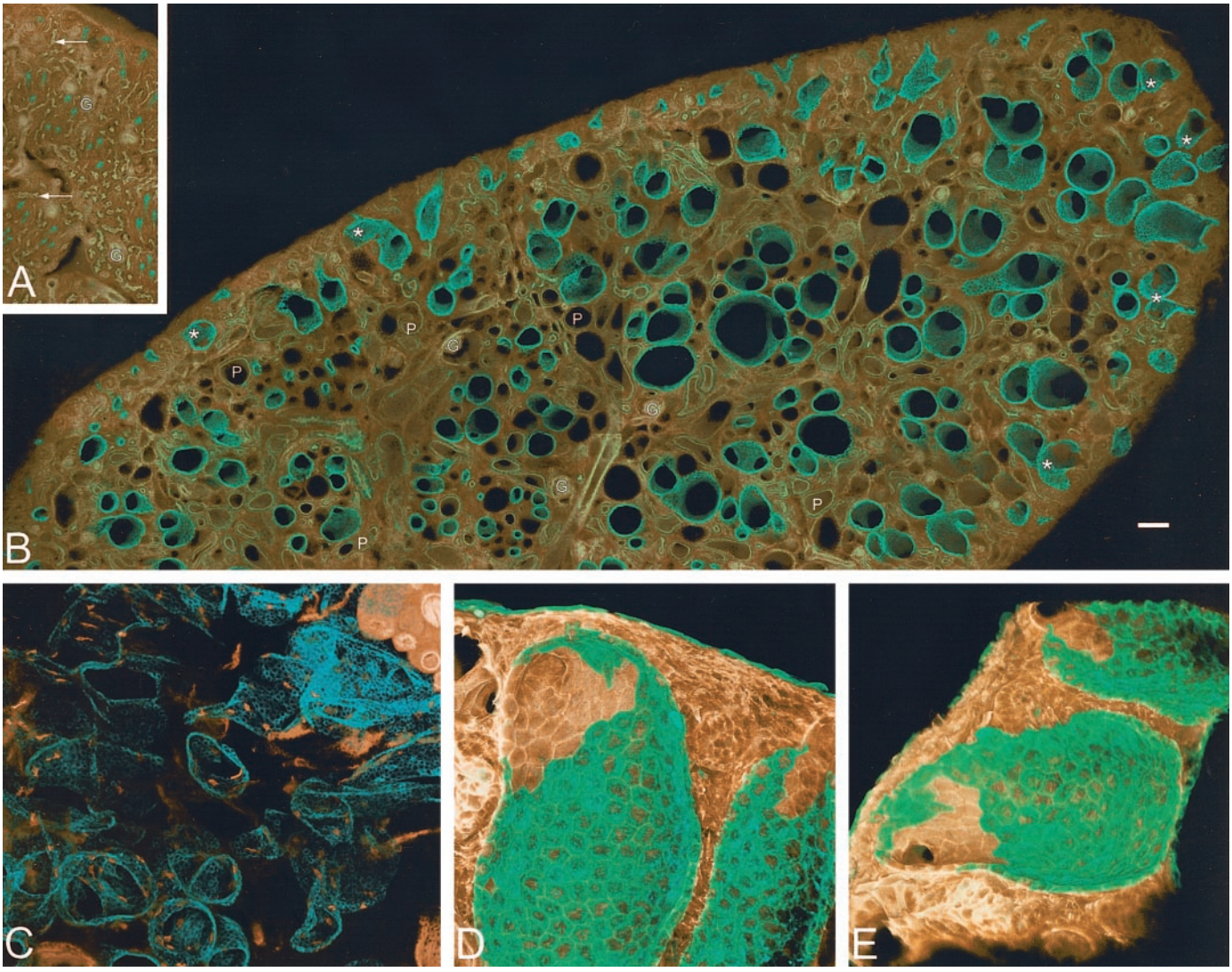

Figure 8. Dual-channel, two-photon microscopy and three-dimensional renderings of collecting ducts (DBA lectin, green). (A) Day P5 +/+ with phalloidin (tan); image assembled from 2 adjacent Z-series; arrows point to proximal tubules; G = glomerulus. (B) Day P5 *inv/inv* with phalloidin (tan); collecting duct cysts with focal absence of DBA labeling at proximal ends are indicated with an asterix; P = proximal tubules with visible apical brush borders; image assembled from 28 adjacent Z-series. Scale bar for A and B = 100 μm. (C) Day P2 *inv/inv* collecting ducts with LTG-lectin checkerboard labeling of intercalated cells (tan) against DBA-positive principal cells (green); assembled from 4 adjacent Z-series. (D, E) Day P5 *inv/inv* with phalloidin (tan), 205 × 205 × 50 μm volume is presented in different rotations to emphasize heterogeneous labeling of epithelial cells within single cysts.

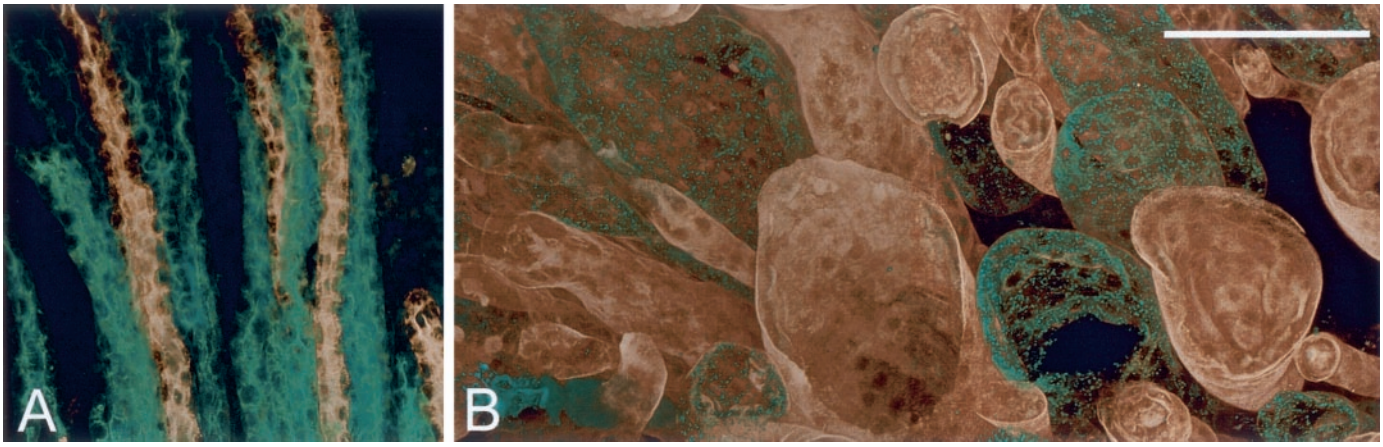

Figure 9. Dual-color, two-photon microscopy and three-dimensional rendering of day P5 +/+ (A) and *inv/inv* (B) outer medulla. Thick ascending limbs labeled with anti–Tamm-Horsfall (green) run parallel to DBA-positive collecting ducts (brown). Panel A was collected over a depth of 30 μm (single Z-series). Panel B was collected over 64 μm (two adjacent Z-series). Scale bar for A and B = 100 μm.

brane, we were able to identify the normal arrangement of nine peripheral doublet microtubules around a central pair (9 + 2). Neighboring cilia showed parallel alignment of ciliary axes (data not shown) (37).

Discussion

The study presented here provides the first comprehensive analysis of cyst development and progression in kidneys of *inv/inv* mice. We observed a steady progression of corticomedullary cysts in *inv/inv* kidneys from embryonic day 15 to postpartum day 11 in a pattern resembling NPHP in humans. NPHP is characterized by corticomedullary cysts, thickening and attenuation of tubular basement membranes, tubular atrophy, periglomerular and interstitial fibrosis, and round cell infiltrates in the interstitium (7,38). In familial juvenile NPHP1, Sherman *et al.* (39) described cysts in collecting ducts and distal convoluted tubules, and diverticula involving loops of Henle and the distal nephron. Gagnadoux *et al.* (40) proposed an infantile variant of NPHP when describing diffuse chronic tubulointerstitial nephritis characterized by microcystic dilatation of proximal tubules and Bowman's space in seven infants who progressed to end-stage renal disease (ESRD) before age 2 yr. The suggestion that infantile NPHP may be associated with *INVS* was found in a Bedouin family with a mutation on chromosome 9q22–31, the synthenic region for murine *Invs* (41). This family was studied by Otto *et al.* (7), who reported *Invs* in mice is orthologous to human *NPHP2*, having identified nine distinct recessive mutations in seven families with NPHP2. All patients developed ESRD by 5 yr of age; three families had documented renal cysts and one patient had *situs inversus*.

Early reports of *inv/inv* mice described cysts only in collecting ducts of newborns (24,27). We show cysts in collecting ducts, proximal tubules, thick ascending limbs, and Bowman's capsules that steadily progress from embryonic through newborn development. Normal and narrowed segments are identified within individual proximal tubules. Descending thin loops of Henle show narrowing and focal diverticula. Newborn *inv/inv* mice develop severe azotemia and most succumb to renal failure within 1 wk, consistent with the rapid disease progression reported in infantile NPHP2. However, we did not observe tubular atrophy and interstitial fibrosis described in NPHP2 because this chronicity is not likely to manifest during the short life span of *inv/inv* mice.

At E15 the most mature, deep cortical glomeruli show dilation of Bowman's capsule. By E17, proximal tubule cysts develop in association with the more numerous collecting duct cysts. Although collecting ducts may appear haphazardly arranged in 2-D, our 3-D imaging shows *inv/inv* collecting ducts run parallel along their expected linear path from medulla to cortex. During maturation these ducts uniformly dilate throughout their lengths except at their proximal immature tips in the superficial cortex. Cysts in *inv/inv* collecting ducts and proximal tubules are predominantly fusiform with rare lateral out-pocketing of renal tubule epithelial cells. Although isolated blind pouches were not identified, our segmentation of proximal tubule lumina did identify cysts bridged by narrowed segments that may function as blind pouches. Proximal tubules and collecting ducts from *cpk* mice also exhibit fusiform dilation while undergoing cystogenesis (32,33). Out-pocketing of renal tubular epithelial cells in the pathogenesis of renal cysts is associated with human ADPKD (34) and is thought to be the result of loss of heterozygosity in the clonal cell that gives rise to a cyst. However, loss of heterozygosity in individual somatic cells is not required for cyst formation in ARPKD or NPHP in humans or mice, including *inv/inv*, because all cells in these cystic kidneys inherit two copies of the mutated gene.

inv/inv kidneys showed complexity in shape and cellular composition of cysts. First, in proximal tubules, fusiform cysts are contiguous with either normal or narrow segments similar to linked sausages. Normal caliber tubule segments are found between the fusiform cysts in the *cpk* model (33). Because all cells inherit two mutated genes and only portions of proximal tubules develop cysts, there may be local factors contributing to cyst formation in *inv/inv* and possibly in humans and other murine models with inherited cystic renal diseases. Second,

individual collecting duct cysts in *inv/inv* newborns contain a mixture of both principal and intercalated cells in a distribution pattern similar to +/+. This suggests that, in the *inv/inv* model, collecting duct cysts do not arise from clonal proliferation of a single mutated principle or intercalated cell because we did not identify collecting duct cysts composed entirely of DBA-positive principle cells or DBA-negative intercalated cells.

Finally, we found that one cyst potentially may involve contiguous but heterogeneous tubule segments, such as cystic collecting ducts that uniformly lack DBA staining at the tran-

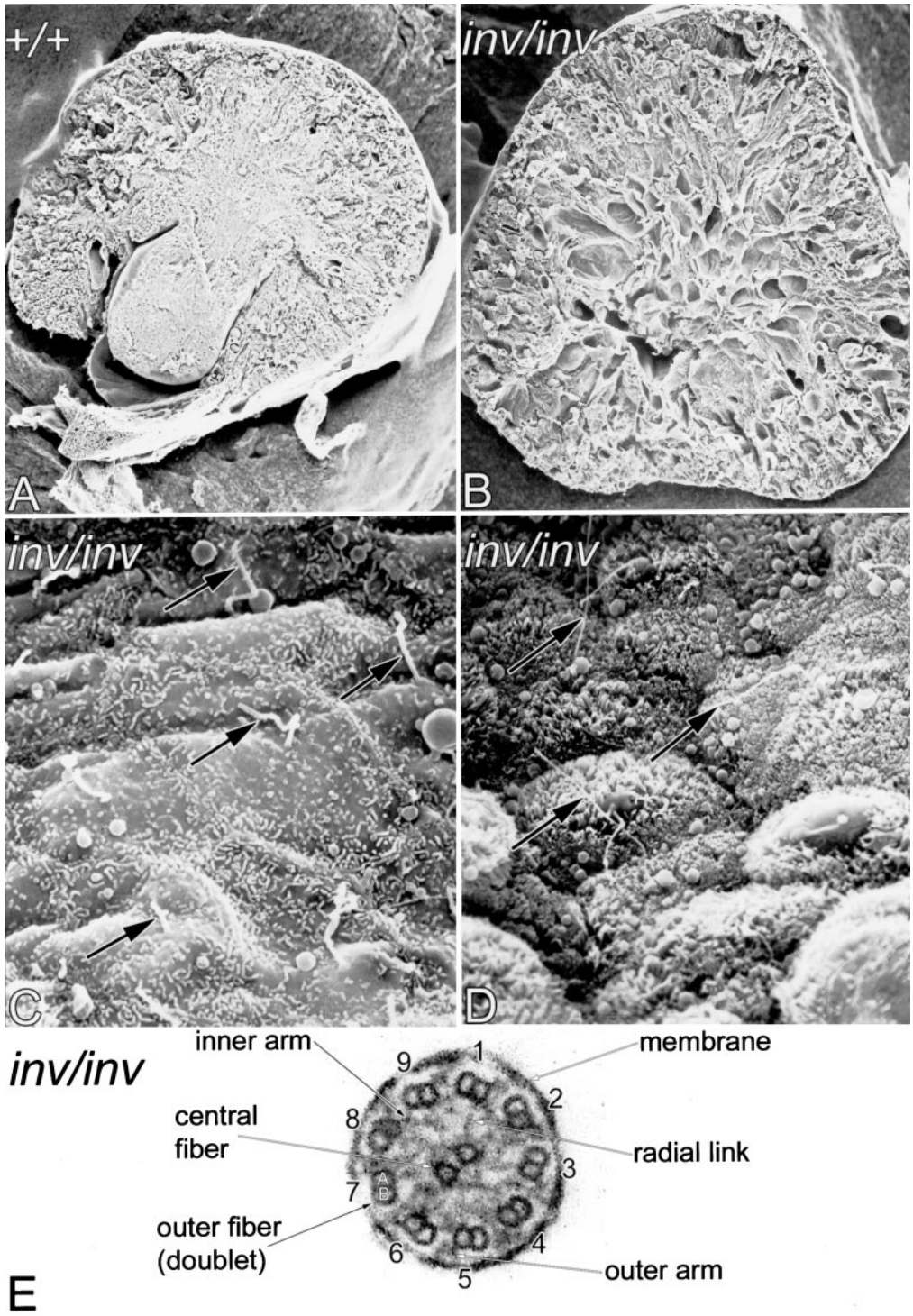

Figure 10. Scanning and transmission electron microscopy of day P5 cilia. (A) +/+ kidney (original magnification, ×40). (B) *inv/inv* kidney (original magnification, ×35). (C) *inv/inv* outer cortical collecting duct (original magnification, ×5500). (D) *inv/inv* proximal tubule (original magnification, ×3500). Cilia on apical surfaces are indicted with arrows. (E) Cross section of 9 + 2 respiratory cilium in *inv/inv* mouse trachea (original magnification, ×52,000).

sition to distal connecting segments. Alternatively, this heterogeneous staining pattern may not represent one cyst formed across two distinct tubule segments but may in fact represent the loss of DBA staining in one cystic collecting duct. We favor the former explanation given the sharply demarcated staining pattern consistently lost at distal connecting segments (future distal convoluted tubules) of both cystic and normal collecting ducts.

The diversity of cystic animal models suggests many proteins interact to ensure tubule integrity. Currently available murine models with PKD and NPHP (1) have supported the concept that many gene mutations may be responsible for cystogenesis. The *inv* mouse represents one model with renal cysts similar to human and other murine forms of ARPKD and NPHP but also has left-right asymmetry defects and cardiopulmonary (29) and hepatobiliary pathology (28). Cilia are postulated to establish left-right asymmetry (14) and have been implicated in renal cystogenesis (15). During early embryonic mouse development, asymmetrical currents generated by the vortical motion of nodal cilia are believed to establish the left-right axis. Praetorius and Spring (42) mechanically bent monocilia of cultured Madine Darby canine kidney (MDCK) cells and detected increased intracellular calcium that propagated as a wave from the perturbed cell to neighboring cells by diffusion of a second messenger via gap junctions.

The first connection of cilia to cysts was found in studies of *TgN737Rpw* that is mutated in *orpk* mice. Partial deletion of *TgN737Rpw* results in cystic kidneys (43), but mice with *Tg737*Δ2–3bGal knockout allele have left-right asymmetry and defective cilia (44). *Polaris*, the product of *TgN737Rpw*, has been localized to axoneme of MDCK cilia (21), suggesting an intact cilia function is required for renal and axis development. Cystin, encoded by *Cys1* and defective in *cpk* mice, is found in cilia (18). Although cysts of *inv/inv* exhibit structurally normal nonmotile cilia similar to the *cpk* mouse, functionally *inv/inv* motile cilia have been reported to generate slow, turbulent nodal flow (45). A subset of motile cilia containing left-right dynein appears to generate nodal flow that is sensed by nonmotile cilia containing polycystin-2 (46). Patients with ADPKD who inherit a *PKD2* mutation have defective polycystin-2 but normal left-right axis (2). Individuals with *situs inversus* due to a defect in ciliary dynein arms do not develop renal cysts (15), and therefore, just having nonfunctional motile cilia cannot cause cysts. How defective cilia induce NPHP is unclear; however, data from several models clearly implicate ciliary function in the pathogenesis of renal cystic disease. The *inv/inv* mouse will be useful for the study of cilia defects and appears to represent a good model system for early infantile nephronophthisis.

Acknowledgments

We thank Michael Goheen, Barry Babin, Michael Sanford, Olga Cabello, and Doug Kojetin for technical assistance and Heather Ward for reading the manuscript. Figures were prepared with the assistance of Jill Goodwin and Brent Gann. C.L.P. acknowledges NIH K08 DK02785, Polycystic Kidney Disease Foundation grant 99023, National Kidney Foundation of Indiana, Indiana University School of Medicine Biomedical Research Grant, Clarian Health Values Fund VFR21, and Ralph W. and Grace M. Showalter Foundation. Funds were also received from Deutsche Forschungsgemeinschaft (J.N.), NIH PO1 HL49953 (P.A.O.), Indiana University Strategic Directions Initiative (K.W.D.), and the Indiana Genomics Initiative grant from the Lilly Foundation to Indiana University School of Medicine. Parts of this manuscript were presented in poster form at the national meetings of the American Society of Nephrology and the American Society for Cell Biology.

References

1. Guay-Woodford LM: Murine models of polycystic kidney disease: Molecular and therapeutic insights. *Am J Physiol Renal Physiol* 285: F1034–F1049, 2003
2. Harris PC: Molecular basis of polycystic kidney disease: PKD1, PKD2 and PKHD1. *Curr Opin Nephrol Hypertens* 11: 309–314, 2002
3. Johnson CA, Gissen P, Sergi C: Molecular pathology and genetics of congenital hepatorenal fibrocystic syndromes. *J Med Genet* 40: 311–319, 2003
4. Ward CJ, Yuan D, Masyuk TV, Wang X, Punyashthiti R, Whelan S, Bacallao R, Torra R, LaRusso NF, Torres VE, Harris PC: Cellular and subcellular localization of the ARPKD protein: Fibrocystin is expressed on primary cilia. *Hum Mol Genet* 12: 2703–2710, 2003
5. Onuchic LF, Furu L, Nagasawa Y, Hou X, Eggermann T, Ren Z, Bergmann C, Senderek J, Esquivel E, Zeltner R, Rudnik-Schoneborn S, Mrug M, Sweeney W, Avner ED, Zerres K, Guay-Woodford LM, Somlo S, Germino GG: *PKHD1*, the polycystic kidney and hepatic disease 1 gene, encodes a novel large protein containing multiple immunoglobulin-like plexin-transcription-factor domains and parallel beta-helix 1 repeats. *Am J Hum Genet* 70: 1305–1317, 2002
6. Hildebrandt F, Otto E, Rensing C, Nothwang HG, Vollmer M, Adolphs J, Hanusch H, Brandis M: A novel gene encoding an SH3 domain protein is mutated in nephronophthisis type 1. *Nat Genet* 17: 149–153, 1997
7. Otto EA, Schermer B, Obara T, O'Toole JF, Hiller KS, Mueller AM, Ruf RG, Hoefele J, Beekmann F, Landau D, Foreman JW, Goodship JA, Strachan T, Kispert A, Wolf MT, Gagnadoux MF, Nivet H, Antignac C, Walz G, Drummond IA, Benzing T, Hildebrandt F: Mutations in INVS encoding inversin cause nephronophthisis type 2, linking renal cystic disease to the function of primary cilia and left-right axis determination. *Nat Genet* 34: 413–420, 2003
8. Olbrich H, Fliegauf M, Hoefele J, Kispert A, Otto E, Volz A, Wolf MT, Sasmaz G, Trauer U, Reinhardt R, Sudbrak R, Antignac C, Gretz N, Walz G, Schermer B, Benzing T, Hildebrandt F, Omran H: Mutations in a novel gene, *NPHP3*, cause adolescent nephronophthisis, tapeto-retinal degeneration and hepatic fibrosis. *Nat Genet* 34: 455–459, 2003
9. Mollet G, Salomon R, Gribouval O, Silbermann F, Bacq D, Landthaler G, Milford D, Nayir A, Rizzoni G, Antignac C, Saunier S: The gene mutated in juvenile nephronophthisis type 4 encodes a novel protein that interacts with nephrocystin. *Nat Genet* 32: 300–305, 2002
10. Lubarsky B, Krasnow MA: Tube morphogenesis: Making and shaping biological tubes. *Cell* 112: 19–28, 2003
11. Avner ED: Epithelial polarity and differentiation in polycystic kidney disease. *J Cell Sci Suppl* 17: 217–222, 1993

12. Calvet JP: Polycystic kidney disease: Primary extracellular matrix abnormality or defective cellular differentiation? *Kidney Int* 43: 101–108, 1993
13. Woo D: Apoptosis and loss of renal tissue in polycystic kidney diseases. *N Engl J Med* 333: 18–25, 1995
14. McGrath J, Brueckner M: Cilia are at the heart of vertebrate left-right asymmetry. *Curr Opin Genet Dev* 13: 385–392, 2003
15. Igarashi P, Somlo S: Genetics and pathogenesis of polycystic kidney disease. *J Am Soc Nephrol* 13: 2384–2398, 2002
16. Watanabe D, Saijoh Y, Nonaka S, Sasaki G, Ikawa Y, Yokoyama T, Hamada H: The left-right determinant Inversin is a component of node monocilia and other 9+0 cilia. *Development* 130: 1725–1734, 2003
17. Morgan D, Eley L, Sayer J, Strachan T, Yates LM, Craighead AS, Goodship JA: Expression analyses and interaction with the anaphase promoting complex protein Apc2 suggest a role for inversin in primary cilia and involvement in the cell cycle. *Hum Mol Genet* 11: 3345–3350, 2002
18. Hou X, Mrug M, Yoder BK, Lefkowitz EJ, Kremmidiotis G, D'Eustachio P, Beier DR, Guay-Woodford LM: Cystin, a novel cilia-associated protein, is disrupted in the *cpk* mouse model of polycystic kidney disease. *J Clin Invest* 109: 533–540, 2002
19. Taulman PD, Haycraft CJ, Balkovetz DF, Yoder BK: Polaris, a protein involved in left-right axis patterning, localizes to basal bodies and cilia. *Mol Biol Cell* 12: 589–599, 2001
20. Pazour GJ, San Agustin JT, Follit JA, Rosenbaum JL, Witman GB: Polycystin-2 localizes to kidney cilia and the ciliary level is elevated in orpk mice with polycystic kidney disease. *Curr Biol* 12: R378–R380, 2002
21. Yoder BK, Hou X, Guay-Woodford LM: The polycystic kidney disease proteins, polycystin-1, polycystin-2, polaris, and cystin, are co-localized in renal cilia. *J Am Soc Nephrol* 13: 2508–2516, 2002
22. Huan Y, van Adelsberg J: Polycystin-1, the PKD1 gene product, is in a complex containing E-cadherin and the catenins. *J Clin Invest* 104: 1459–1468, 1999
23. Nurnberger J, Bacallao RL, Phillips CL: Inversin forms a complex with catenins and N-cadherin in polarized epithelial cells. *Mol Biol Cell* 13: 3096–3106, 2002
24. Mochizuki T, Saijoh Y, Tsuchiya K, Shirayoshi Y, Takai S, Taya C, Yonekawa H, Yamada K, Nihei H, Nakatsuji N, Overbeek PA, Hamada H, Yokoyama T: Cloning of *inv*, a gene that controls left/right asymmetry and kidney development. *Nature* 395: 177–181, 1998
25. Lowe LA, Supp DM, Sampath K, Yokoyama T, Wright CV, Potter SS, Overbeek P, Kuehn MR: Conserved left-right asymmetry of nodal expression and alterations in murine *situs inversus*. *Nature* 381: 158–161, 1996
26. Yokoyama T, Copeland NG, Jenkins NA, Montgomery CA, Elder FF, Overbeek PA: Reversal of left-right asymmetry: A *situs inversus* mutation. *Science* 260: 679–682, 1993
27. Morgan D, Turnpenny L, Goodship J, Dai W, Majumder K, Matthews L, Gardner A, Schuster G, Vien L, Harrison W, Elder FF, Penman-Splitt M, Overbeek P, Strachan T: Inversin, a novel gene in the vertebrate left-right axis pathway, is partially deleted in the *inv* mouse. *Nat Genet* 20: 149–156, 1998
28. Mazziotti MV, Willis LK, Heuckeroth RO, LaRegina MC, Swanson PE, Overbeek PA, Perlmutter DH: Anomalous development of the hepatobiliary system in the *Inv* mouse. *Hepatology* 30: 372–378, 1999
29. Morishima M, Yasui H, Nakazawa M, Ando M, Ishibashi M, Takao A: Situs variation and cardiovascular anomalies in the transgenic mouse insertional mutation, *inv*. *Teratology* 57: 302–309, 1998
30. Schon P, Tsuchiya K, Lenoir D, Mochizuki T, Guichard C, Takai S, Maiti AK, Nihei H, Weil J, Yokoyama T, Bouvagnet P: Identification, genomic organization, chromosomal mapping and mutation analysis of the human *INV* gene, the ortholog of a murine gene implicated in left-right axis development and biliary atresia. *Hum Genet* 110: 157–165, 2002
31. Phillips CL, Arend LJ, Filson AJ, Kojetin DJ, Clendenon JL, Fang S, Dunn KW: Three-dimensional imaging of embryonic mouse kidney by two-photon microscopy. *Am J Pathol* 158: 49–55, 2001
32. Avner ED, Studnicki FE, Young MC, Sweeney WE Jr, Piesco NP, Ellis D, Fettermann GH: Congenital murine polycystic kidney disease. I. The ontogeny of tubular cyst formation. *Pediatr Nephrol* 1: 587–596, 1987
33. Gattone VH, 2nd, Calvet JP, Cowley BD Jr, Evan AP, Shaver TS, Helmstadter K, Grantham JJ: Autosomal recessive polycystic kidney disease in a murine model: A gross and microscopic description. *Lab Invest* 59: 231–238, 1988
34. Potter EL: *Normal and Abnormal Development of the Kidney*. Chicago, Year Book Medical Publishers, pp 124–130, vii-viii, 1972
35. Ricker JL, Gattone VH 2nd, Calvet JP, Rankin CA: Development of autosomal recessive polycystic kidney disease in BALB/c-cpk/cpk mice. *J Am Soc Nephrol* 11: 1837–1847, 2000
36. Clendenon JL, Phillips CL, Sandoval RM, Fang S, Dunn KW: Voxx: A PC-based, near real-time volume rendering system for biological microscopy. *Am J Physiol Cell Physiol* 282: C213–C218, 2002
37. Rutland R, Morgan L, Waters KA, van Asperen P, de longh RU: Diagnosis of primary ciliary dyskinesia. In: *Cilia, Mucus, and Mucociliary Interactions*, Vol. 1, edited by Baum GL, Priel Z, Roth Y, Liron N, Pstfeld EJ, New York, Marcel Dekker, pp 407–428, 1998
38. Hildebrandt F, Omram H: New insights: Nephronophthisis-medullary cystic kidney disease. *Pediatr Nephrol* 16: 168–176, 2001
39. Sherman FE, Studnicki FM, Fetterman G: Renal lesions of familial juvenile nephronophthisis examined by microdissection. *Am J Clin Pathol* 55: 391–400, 1971
40. Gagnadoux MF, Bacri JL, Broyer M, Habib R: Infantile chronic tubulointerstitial nephritis with cortical microcysts: Variant of nephronophthisis or new disease entity? *Pediatr Nephrol* 3: 50–55, 1989
41. Haider NB, Carmi R, Shalev H, Sheffield VC, Landau D: A Bedouin kindred with infantile nephronophthisis demonstrates linkage to chromosome 9 by homozygosity mapping. *Am J Hum Genet* 63: 1404–1410, 1998
42. Praetorius HA, Spring KR: Bending the MDCK cell primary cilium increases intracellular calcium. *J Membr Biol* 184: 71–79, 2001
43. Yoder BK, Richards WG, Sommardahl C, Sweeney WE, Michaud EJ, Wilkinson JE, Avner ED, Woychik RP: Functional correction of renal defects in a mouse model for ARPKD through expression of the cloned wild-type Tg737 cDNA. *Kidney Int* 50: 1240–1248, 1996
44. Murcia NS, Richards WG, Yoder BK, Mucenski ML, Dunlap JR, Woychik RP: The Oak Ridge Polycystic Kidney (*orpk*) disease gene is required for left-right axis determination. *Development* 127: 2347–2355, 2000
45. Okada Y, Nonaka S, Tanaka Y, Saijoh Y, Hamada H, Hirokawa N: Abnormal nodal flow precedes *situs inversus* in *iv* and *inv* mice. *Mol Cell* 4: 459–468, 1999
46. McGrath J, Somlo S, Makova S, Tian X, Brueckner M: Two populations of node monocilia initiate left-right asymmetry in the mouse. *Cell* 114: 61–73, 2003